Brain Research Bulletin 88 (2012) 189–198

Contents lists available at ScienceDirect

Brain Research Bulletin

journal homepage: www.elsevier.com/locate/brainresbull

Research report

Light and electron microscopic characterization of the evolution of cellular pathology in the Hdh$^{(CAG)150}$ Huntington's disease knock-in mouse☆

Zubeyde Bayram-Weston[a,*], Eduardo M. Torres[a], Lesley Jones[b], Stephen B. Dunnett[a], Simon P. Brooks[a]

[a] School of Biosciences, Cardiff University, Museum Avenue, Cardiff CF10 3AX, Wales, UK
[b] Department of Psychological Medicine, 2nd Floor, Henry Wellcome Building, Wales School of Medicine, Cardiff University, Cardiff CF14 4XN, Wales, UK

ARTICLE INFO

Article history:
Received 29 July 2010
Received in revised form 15 March 2011
Accepted 18 March 2011
Available online 13 April 2011

Keywords:
Huntington's disease
Aggregations
Inclusions
HdhQ150/Q150
Knock-in
Transmission electron microscope (TEM)

ABSTRACT

Huntington's disease is an autosomal dominant, progressive neurodegenerative disease in which a single mutation in the gene responsible for the protein huntingtin leads to a primarily striatal and cortical neuronal loss, resulting progressive motor, cognitive and psychiatric disability and ultimately death. The mutation induces an abnormal protein accumulation within cells, although the precise role of this accumulation in the disease process is unknown. Several animal models have been created to model the disease. In the present study, the pathology of the *Hdh*$^{CAG(150)}$ mouse model was analyzed longitudinally over 24 months. At 5 months of age, the mutant N-terminal antibody S830 found dense nuclear staining and nuclear inclusions in the olfactory tubercle and striatum of the *Hdh*$^{Q150/Q150}$ mice. Nuclear inclusions increased in number and size with age and disease progression, and spread in ventral to dorsal, and anterior to posterior pattern. Electron microscopy observations at 14 months of age revealed that the neurons showed a normal nucleus having a circular shape and regular membranes in a densely packed cytoplasm, whereas by 21 months the cytoplasm was vacuolated and contained swollen mitochondria with many degenerated cytoplasmic organelles. Immunogold labelling of the S830 antibody was found to be specifically localised to the inner area of the neuronal intra-nuclear inclusions.

Our data demonstrate a marked and progressive cellular phenotype that begins at 5 months of age and progresses with time. The pathology the *Hdh*$^{Q150/Q150}$ line was focused on the striatum and cortex until the late stage of the disease, consistent with the human condition.

© 2011 Elsevier Inc. All rights reserved.

1. Introduction

Huntington's disease (HD) is an adult-onset neurodegenerative disorder characterized by progressive cognitive, psychiatric and motor symptoms. It is associated with a mutation in the *htt gene*, which codes for the huntingtin protein (Htt). The gene contains a polymorphic stretch of repeated CAG trinucleotides which encodes polyglutamine (polyQ) [40]. Mutant htt contains an abnormal CAG repeat expansion responsible for the neurodegeneration, primary focus on the basal ganglia and cerebral cortex [45], which may be preceded by neuronal dysfunction. The most noticeable neurodegenerative changes are found in the medium spiny neurons (MSNs) of striatum (caudate nucleus and putamen) with neuronal loss and astrogliosis being a feature [2,44,45]. In addition to this severe loss of the MSNs, some atrophy is also present in the cerebral cortex [19,31]. As the disease progresses, neuronal loss becomes widespread and effects other regions of the brain linked to corticostriatal circuits, including the globus pallidus (GP), thalamus, substantia nigra (SN) and hippocampus [9,44,45]. How the mutated huntingtin protein causes this cell death is still a matter of speculation.

In HD, mutant huntingtin misfolds and accumulates as large insoluble aggregates/neuronal intra-nuclear inclusions (NIIs). These NIIs are a pathological marker of the disease both in mice and humans [7,8]. The expanded CAG sequence of mutant huntingtin causes protein misfolding and promotes the recruiting of a variety of proteins which then form aggregates [7,8,14]. Although, the genetics of HD are well documented, the functional role of protein aggregation in neuronal cell death remains unclear. It is still unknown as to whether aggregates are toxic to neurons, protective against cell degeneration, or simply a side-product markers of other ongoing cellular processes causing cell death [27,32,34,37].

In addition to the NII pathology within the cell soma, it has also been observed that N-terminal fragments of mutant huntingtin accumulate in dystrophic neurites in the cortex, the striatum and in astrocytes in the R6/2 transgenic mice [35,42], and in post mortem HD brains [32,36]. Extra-nuclear neuronal inclusions (ENNIs) have been identified in both human and mouse brain [8,15,22]. These ENNIs may be the precursors of intra-nuclear inclusions [18].

☆ This article is part of a Special issue entitled 'HD Transgenic Mouse'.

* Corresponding author. Tel.: +44 29 20 874684; fax: +44 29 20 876749.
E-mail address: bayram-westonZ@cardiff.ac.uk (Z. Bayram-Weston).

0361-9230/$ – see front matter © 2011 Elsevier Inc. All rights reserved.
doi:10.1016/j.brainresbull.2011.03.014

Gutekunst et al. [11] found that neuropil aggregates were much more common than nuclear aggregates and they were present before the onset of clinical symptoms in post mortem HD brains.

A third key sign of cellular pathology is the astrocyte-mediated inflammatory response to cell insult. Glial fibrillary acidic protein (GFAP) is expressed primarily by astroglia and is an indicator of astroglial activation [3,6,28]. The brain reacts to neuronal injuries with an increase in number and size of cells expressing GFAP [48]. Astrogliosis is observed in human HD [10,43] and in the HD mouse lines including $Hdh^{CAG(150)}$ [17] and HD89 [26]. By contrast, other mouse lines, such as R6/2 mice, do not show any reactive astrogliosis, although they do exhibit modest cell death, striatal atrophy, and reduced brain size [20].

The present study sought to characterise the development of disease neuropathology in the $Hdh^{(CAG)150}$ mouse line. We used histology and immunohistochemistry with stereological quantitation, and transmission electron microscopy (TEM) to investigate aggregate formation in more detail in an attempt to better understand the development of neuronal pathology in this mouse model of HD. The present study focused on the progression, distribution, number and form of huntingtin aggregates in the different regions of the brain, and also assessed brain atrophy and neuronal cell loss within the same brain sections from tissue taken at regular intervals between 5 and 24 months of age.

2. Materials and methods

2.1. Animals

In total 99 mice were used in the present study, spread across 9 time points (5 months = 7; 6 months = 11; 8 months = 5; 10 months = 16; 12 months = 12; 15 months = 12; 18 months = 15; 21 months = 10; 24 months = 10). Fifty one of these mice (29 female and 22 male) were $Hdh^{Q150/Q150}$ knock-in mice with 48 wildtype litter mates (29 female and 19 male). The mice were bred in-house from the original line, imported to our laboratory on a mixed 129/Ola × C57BL/6 J background and backcrossed onto C57BL/6 J background (Harlan, UK) over six generations. This mouse has had the normal length CAG repeat in exon 1 of the mouse *Hdh* gene replaced with a 150 CAG repeats [17]. These mice had on average 132 ± 2.65 CAG repeats (range 120–143 repeats). The mice were housed together under standard conditions with *ad libitum* access to water and food. The mice were housed in a holding room under a 12 h:12 h light/dark cycle (lights on 0700 h) and an ambient room temperature of 21 ± 1 °C. The cages contained sawdust bedding and a cardboard tube for environmental enrichment. Each cage contained 2–6 animals. Each mouse had undergone periodic behavioural testing for up to two years [4]. This study was carried out in accordance with the UK Animals (Scientific Procedures) Act, 1986.

2.2. Histology

The animals were sacrificed at 3 months = 3, 5 months = 7; 6 months = 11; 8 months = 5; 10 months = 16; 12 months = 12; 15 months = 12; 18 months = 15; 21 months = 10; 24 months = 10. They were anaesthetized by intraperitoneal injection of 0.2 ml of Euthetal (Merial, Essex, UK) and then perfused intracardially with phosphate-buffered saline (PBS, pH 7.4) for 3 min. Followed by 4% paraformaldehyde (PFA) (Fisher Scientific, Loughborough, UK) in a 0.1 M PBS solution, pH 7.4, for a further 5 min. The brains were carefully removed, post fixed in 4% PFA for 4 h, and then transferred in 25% sucrose in PBS, until they sank. For striatal analysis coronal sections (40 μm) of the brain were cut in series of 1:6 using a freezing sledge microtome (Leitz Bright Series 8000, Germany). The sections were stored in cryoprotective solution at −20 °C.

2.3. Cresyl fast violet (CV)

A one in six series was stained using the standard Nissl stain, cresyl fast violet for morphological and stereological analysis. The sections were mounted on gelatine-coated glass slides (Fisher Scientific), and allowed to dry at 37 °C for 24 h. The sections were then dehydrated in a graded series of ethanol (5 min each, 70%, 95%, and 100%) and delipidised in a mixture of chloroform and ethanol (1:1, v/v) for 20 min. Following delipidisation, the sections were hydrated in a gradually decreasing series of ethanol (5 min each 100%, 95% and 70%) and immersed in distilled water for 5 min and stained with cresyl violet (0.7% in distilled water with 0.5% sodium acetate, Sigma, Hertfordshire, UK) for 5 min. After rinsing in distilled water for 1 min, the sections were dehydrated in a graded series of ethanol (5 min each, 70%, 95%, and 100%), cleared in xylene (VWR, Darmstadt, Germany) for at least for 10 min, cover-slipped with DPX mounting medium (RA Lamb, Hambridge, Somerset, UK) and analyzed under a Leica DMRBE microscope (Leica, Wetzlar, Germany).

2.4. Immunohistochemistry

Immunohistochemistry was carried out according to Trueman et al. [41]. Briefly, all stains were performed on a 1:6 series of sections. Free-floating sections were processed immunohistochemically using the sheep anti-S830 (a kind gift from Prof. Gillian Bates, King's College, London, UK) and rabbit GFAP (DAKO, Cambridge, UK) primary antibodies. The S830 antibody was raised against the product of the N-terminal region to 53 glutamine residues of exon 1 and selectively recognizes the aggregated form of the mutated htt protein [21].

The sections were placed in (pH 7.4) TRIS buffered saline (TBS), and washed twice for 5 min. The endogenous peroxidise activity was inhibited by incubation in methanol containing 3% H_2O_2 (VWR) for 5 min, and then placed in TBS. Non-specific binding sites were blocked with 3% horse serum in TBS for 1 h, and the sections were incubated with S830 antibody (diluted 1:25,000) and GFAP antibody (1:2000) overnight at room temperature. After several washes in TBS, sections were incubated with a horse anti-goat or horse anti-rabbit secondary antibody (diluted 1:200, Vector Laboratories, Burlingame, CA, USA) for 2 h at room temperature. After several washes in TBS, the sections were incubated with a biotin–streptavidin kit according to the manufacturer's instructions (Vector Laboratories). After each incubation, the sections were rinsed in TBS. The peroxidase activity was visualized with 3,3′-diaminobenzidine (DAB) (Sigma–Aldrich, Poole, Dorset, UK). Finally, the sections were mounted on gelatine-coated slides, dehydrated and cover-slipped.

Light microscopic pictures were taken using a Leica DMRBE microscope fitted with a digital camera (Optronics, Goleta, CA, USA) and MagnaFire 1.2 C imaging Software (Goleta, CA, USA). All images were captured using the same parameters and saved on computer for further analysis. Images were adjusted in contrast and brightness only for optimal display with Adobe Photoshop 6.0.

The staining in the homozygote mice was also scored in a semi-quantitative fashion that included the intensity of specific staining in sections: 0 = absent, + = weak nuclear staining present; ++ = diffuse nuclear staining; +++ = few/minimum inclusions; ++++ = many/dense inclusions. Animal numbers each time point was as follows: 5 months = 4; 6 months = 7; 8 months = 4; 10 months = 7; 12 months = 7; 15 months = 6; 18 months = 4; 21 months = 5; 24 months = 7.

2.5. S830/CV stereology

For the stereological assessment 98 animals were used as follows: 5months = 7; 6 months = 11; 8 months = 5; 10 months = 16; 12 months = 12; 15 months = 12; 18 months = 15; 21 months = 10; 24 months = 10. Two dimensional stereology was carried out using a PC-based image analysis software (Olympus C.A.S.T. grid system v1.6.) on a Olympus BX50 microscope (Olympus Optical Co., Ltd., Tokyo, Japan). Cell counts were carried out on a 1:6 series of GFAP, S830-stained, and CV sections, throughout the entire left striatum and then assessed blindly to the experimental groups. Cell counts were performed on a Leica DMRB microscope with the counting objective was at 100× and counting frame area was 265 μm^2 and corrected using the Abercrombie formula [1].

2.6. Transmission electron microscopy (TEM) for morphological study

For the electron microscopy, four mice for each group (aged 14 months and 21 months) were anaesthetized by intraperitoneal injection of 0.2 ml of Euthetal and then perfused with 0.9% NaCl for 3 min, followed by 2% PFA and 2% glutaraldehyde in 0.1 M PBS solution at pH 7.4, for 5 min. After perfusion, the brains were carefully removed and washed in PBS. Tissues were cut into small cubes and transferred into 1% osmium tetroxide for 2 h at +4 °C. After washing with distilled water 4 × 15 min, the samples were stained overnight in 0.5% uranyl acetate at +4 °C. All tissues used for electron microscopy were dehydrated in ascending concentrations of ethanol and fresh propylene oxide, and then infiltrated overnight in a mixture of propylene oxide and araldite resin (1:1, v/v) on a rotary shaker at room temperature. Following resin infiltration, the tissues were embedded in fresh resin for 48 h at 60 °C. Ultrathin sections (60 nm) were cut with a diamond knife on an ultracut-microtome (Reichert-Jung, Leica UK LTD, Milton Keynes, UK). Thin sections were collected on copper mesh grids, counterstained with 2% uranyl acetate for 10 min followed by Reynold's lead citrate for 5 min and examined under a Philips transmission electron microscope (Philips EM 208, Eindhoven, The Netherlands).

2.7. Transmission electron microscopy for immunogold labelling

Two mice for each group (aged 14 months and 21 months) were anaesthetized by intraperitoneal injection 0.2 ml of Euthetal and then perfused with 0.9% NaCl for 3 min. This was followed by 3% PFA and 0.2% glutaraldehyde in 0.1 M PBS solution, pH 7.4, for 5 min, and then with 3% PFA alone at a rate of 15 ml/min. After perfusion the brains were carefully removed and washed in PBS. Relevant region of the brain was cut into small cubes and transferred into a cryoprotective solution (0.05 M PBS, pH 7.4, containing 25% sucrose and 30% glycerol) for 15 min. The tissue was then transferred into methanol in an automated freeze substitution chamber at −80 °C for 48 h (Reichest *EM*AFS, Leica mikrosysteme, Wien, Austria). The methanol was replaced with fresh methanol during the first 2 h at −80 °C. The chamber temperature was then allowed to increase to −50 °C for 88 h. The tissue was then infiltrated by a mixture of Lowicryl HM20 resin and methanol (1:1, v/v) for 90 min at −50 °C,

then infiltrated with a mixture of Lowicryl HM20 resin and methanol (2:1, v/v) for a further 90 min at −50 °C, then transferred into pure Lowicryl HM20 resin overnight at −50 °C. The tissue was then embedded in fresh Lowicryl HM20 resin under UV light for 48 h at −50 °C. The temperature was then increased to 20 °C for 24 h to complete resin polymerisation. Ultra-thin sections (60 nm) were cut with a diamond knife on the ultracut-microtome. Thin sections were collected on pioloform-coated nickel mesh grids and were blocked with drops of PBS containing 3% normal donkey serum, 1% bovine serum albumine, 0.2% Triton-X and 0.1% sodium azide for 45 min at room temperature. The sections were then incubated on drops of sheep polyclonal S830 primary antibody (1:500) overnight at +4 °C. After rinsing in PBS and distilled water, the sections were incubated again in donkey anti-sheep IgG conjugated gold (10 nm, 1:20; BB International, Cardiff, UK) for overnight at +4 °C. After washing in PBS, the grids were counterstained with 2% uranyl acetate for 10 min followed by Reynold's lead citrate for 5 min and examined using a Philips transmission electron microscope.

2.8. Statistical analysis

Statistical analyses were undertaken using two-way ANOVA (Genstat v13.2; VSN International, Hemel Hempstead, UK), in all cases with age as a between-subjects factor. Striatal volume and total striatal cell counts compared Genotype (wildtype vs. $Hdh^{150/150}$) as a second between-subjects factor, whereas cell counts of striatal cells bearing inclusion pathology used type of pathology (diffuse vs. inclusion) as a second within-subjects factor. In view of the large number of age groups with relatively few animals of each genotype at each age, a subsequent analysis was undertaken to determine the age at which overt pathology was significant by repeating the analyses of variance with data blocked into three age bands: young (4, 6 and 8 month), mature (10, 12 and 15 month) and aged (18, 21 and 24 month). Comparisons between different ages and age ranges were corrected for multiple comparisons by the Newman–Keuls test.

3. Results

3.1. Striatal atrophy and neuronal cell counts in the $Hdh^{(CAG)150}$ mouse

We examined the volume of the striatum in $Hdh^{Q150/Q150}$ mice and wildtype littermates from 5 months to 24 months of age. The volume of the striatum was significantly reduced in the $Hdh^{Q150/Q150}$ mice compared with the wildtype mice irrespective of age (Fig. 1A: genotype, $F_{1,74} = 32.44$, $p < 0.001$). There was also a significant age effect (age, $F_{8,74} = 15.93$, $p < 0.01$) and a significant interaction effect between the groups over time (genotype × age, $F_{8,74} = 3.30$, $p < 0.01$), suggesting that $Hdh^{Q150/Q150}$ mice had reduced striatal volume from 6 months of age which remained lower then that of wildtypes from this point onwards. However, in the *post hoc* analysis with mice blocked into three age bands, the two main effects remained highly significant but the interaction term was no longer so ($F_{2,86} = 0.20$,n.s.), suggesting that the above interaction is associated with random variation between a large number of independent small groups.

In the cresyl violet stained sections, stereological analyses revealed a significant increase in striatal cell numbers from 4 months of age until 8 months which then remained stable (Fig. 1B: age, $F_{8,74} = 12.16$, $p < 0.001$). Furthermore, statistical analysis revealed a significant genotype effect (Fig. 1B: genotype, $F_{1,74} = 6.50$, $p < 0.05$) with $Hdh^{Q150/Q150}$ mice showing reduced cell number throughout. However, no interaction effects was found (genotype × age, $F_{8,74} = 0.92$, n.s.). The main effect of genotype remained significant in the blocked *post hoc* analysis.

3.2. Striatal neuronal pathology in the $Hdh^{Q150/Q150}$ mouse

Within the $Hdh^{Q150/Q150}$ brain, S830 staining showed diffuse nuclear staining and nuclear inclusions only in the homozygous mice. There was no S830 staining found in the control animals, indicating that nuclear inclusion formation was dependent on the mutation. In order to establish the onset age, a small sample of 3 mice was examined at 3 months of age. In this sample, no intra-nuclear inclusions were observed in any region of the brain, however, faint nuclear staining was seen throughout the brain. By 5 months of age the S830 antibody demonstrated diffuse nuclear staining and inclusions, the presence of which varied depending on the brain region. A this early age, diffuse nuclear staining and a low density of inclusions (minimum inclusions) were observed in the olfactory tubercle, central amygdala and striatum (Figs. 2 and 3), but were not apparent in other regions of the brain (Fig. 2 and Table 1). At 15 month of age, nuclear inclusions were distributed widely throughout the brain. At this age persistent diffuse nuclear staining was still present but had disappeared completely by 18 months of age (Fig. 2 and Table 1). In aged homozygous mice (21 and 24 months old), the spatial distribution pattern of inclusions persisted. Analyses of this pathology found that the total number of affected neurons, which was comprised of the collective number of cells with diffuse *htt* staining or inclusions (Fig. 1C: affected neurons, $F_{8,43} = 8.35$, $p < 0.001$) increased up to 18 months of age, before dropping. The number of diffusely stained cells were maximal at the earliest time point investigated at 5 months, and declined thereafter to almost 0 by 18 months of age (Fig. 1D: diffuse staining, $F_{8,43} = 73.00$, $p < 0.001$).

By contrast, the numbers of intra-nuclear inclusions increased to a peak at 18 months of age, before dropping (Fig. 1D: inclusions, $F_{8,43} = 19.54$, $p < 0.001$). Nuclear inclusions appeared to be large, singular and round in one year old mice (Fig. 4C). Inclusions were usually localised in close proximity to the nuclear membrane in older mice (Fig. 4E).

Both the decline of early onset diffuse staining (young > mature > aged) and the increase in the numbers of cells bearing overt inclusions with age (young < mature = aged) remained significant in the blocked analyses ($F_{2,49} = 145.26$ and 29.48, respectively, both $p < 0.001$).

Extra-nuclear inclusions existed in all age groups except 3 month old mice. The distribution of extra-nuclear inclusions was consistent at low levels throughout the brain up to 10 months old. However, by 12 months of age the density of the distribution varied depending on the region of the brain. At this point, the extra-nuclear inclusions increased in the globus pallidus, amygdala and piriform cortex, whereas other area of the brain remained unchanged. In very old homozygous mice (21 and 24 months old), the extra-nuclear inclusions were present throughout the brain (Table 2). Hence, cytosolic and nuclear inclusions increased in number and size with age and disease progression.

3.3. Assessment of neuronal cell death

3.3.1. GFAP immunostaining

GFAP is the main intermediate filament in astrocytes and defines the astrocytic morphology. Since one of the main features of astroglial reaction is the increased size of cellular projections, it is possible to assess the astroglial reaction that is identifiable by the increased expression of GFAP [3]. The expression of GFAP was intense in several regions of the brain including the striatum and cortex (Fig. 5) and increased in the striatum with age in both mouse groups (age, $F_{2,21} = 14.78$, $p < 0.001$), but no differences in expression levels between the groups was identified in either brain region (genotype, $F_{2,21} = 0.69$, n.s.). No interaction effects (genotype × age, $F_{2,21} = 0.95$, n.s.) were found for the expression levels in the striatum (data not shown).

3.4. Electron microscopy

The neurodegeneration of $Hdh^{Q150/Q150}$ knock-in mice at different time points was studied using electron microscopy. Observations of the earlier time point (14 months) revealed that the neurons had a normal circular nucleus with regular membranes, and a densely packed cytoplasm (Fig. 6A). Mitochondria also appeared normal and there was no evidence of vacuolisation,

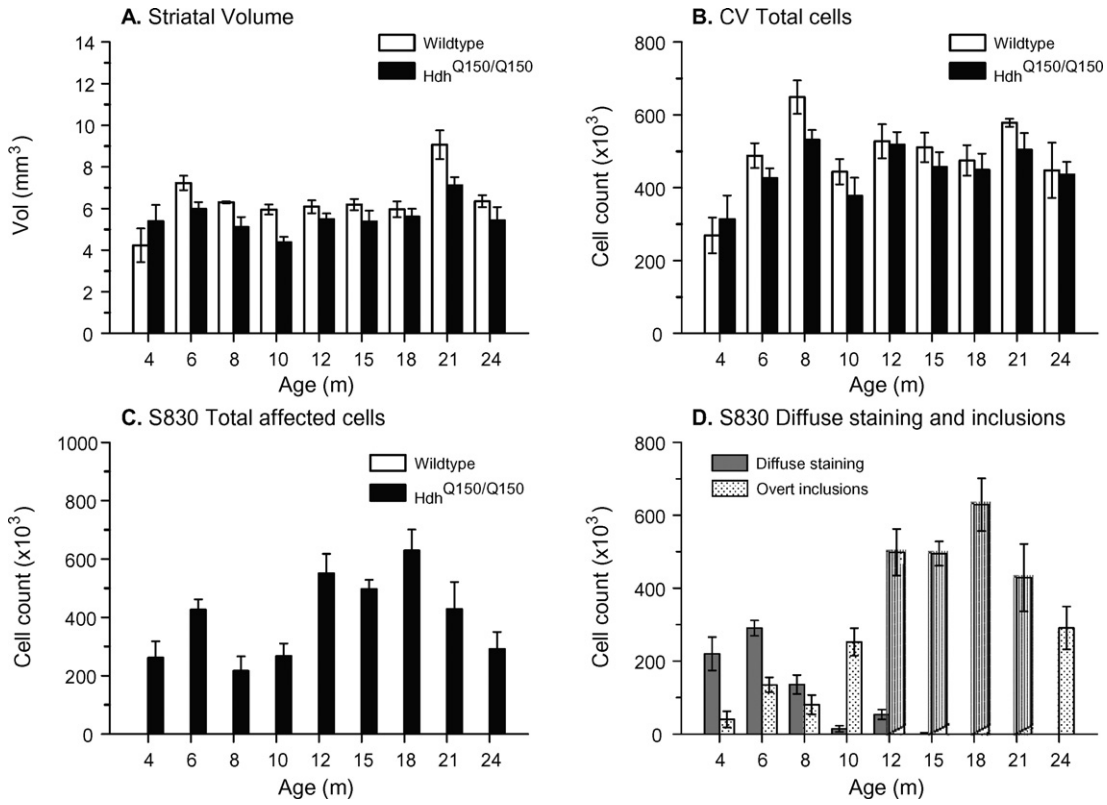

Fig. 1. Age-dependent distribution of cresyl violet – stained neurons and S830 affected cells in striatum of Wt and homozygote. (A) The comparison of the total volume of the striatum in *Hdh*$^{Q150/Q150}$ animals and wildtype mice. In 10 months and 24 months old animals, the volume of the striatum in *Hdh*$^{Q150/Q150}$ animals were less than in wildtype mice. (B) Cresyl violet-stained neurons in both wildtype and homozygote animals. The number of neurons in wildtype is relatively higher than that in homozygotes regardless of age. (C) Age related distribution of S830 affected neurons in striatum of *Hdh*$^{Q150/Q150}$ mice. The number of affected cells increased as age progress from 5 months, peaks at 18 months and gradually decreased thereafter. Affected cells (D) showing diffuse nucleus staining and/or intra-nuclear inclusions. Affected cells showing diffuse nucleus staining decreased in number from 5 months to 12 months, whereas those with intra-nuclear inclusions increased gradually up to age of 18 months and then slowly decreased. Bars indicate means ± s.e.m.

dilation or membrane degeneration. In the *Hdh*$^{Q150/Q150}$ mice, the striatum showed NIIs with a small circular filamentous structure that could be easily identified and clearly distinguishable from the surrounding structures (Fig. 6B). The striatum of the 21 month old wildtype mouse revealed a more compact structure than that of the homozygote animal. That of the 21 month old homozygote showed hypertrophic degenerative neurons with a number of necrotic features (Fig. 6E). These neurons showed structural abnormalities such as angular shape and uneven nuclear membranes. The cytoplasm appeared severely vacuolated and contained swollen mitochondria. Most of the other cytoplasmic organelles were largely deformed. Electron dense bodies were also found in the cytoplasm which may be the degenerated lysosomal structures. However, it is noteworthy that the wildtype mice also showed these bodies but their numbers were reduced from those in the aged matched homozygote mouse. Moreover, the 21 month old

Table 1
Hdh$^{Q150/Q150}$ knock-in mice. Formation, progression and distribution of neuronal intra-nuclear inclusions (NIIs).

Q150 brain/ages	5M	6M	8M	10M	12M	15M	18M	21M	24M
Olfactory tubercle	++/+++	+++	++	++++	++++	++++	++++	++++	++++
Nucleus accumbens	++/+++	+++	++	++++	++++	++++	++++	++++	++++
Globus pallidus-lateral	+/++	+/++	++	+/++	+++	+++	+++	++++	++++
Globus pallidus-medial	+/++	+/++	++	+/++	+++	+++	+++	++++	++++
Striatum ventral	++/+++	+++	+++	++++	++++	++++	++++	++++	++++
Striatum dorsal	++/+++	+++	+++	++++	++++	++++	++++	++++	++++
Striatum posterior	++/+++	+++	+++	++++	++++	++++	++++	++++	++++
Septum lateral	+/++	++	++	++	++	++	+++	++++	+++
Septum med	+/++	++	++	+++	+++	+++	++++	++++	+++
Amygdala BL	+	+	+	+	++	++	+++	+++	+++
Amygdala CL	++/+++	++/+++	++/+++	+++	++++	++++	++++	++++	++++
Thalamus	+/++	++	+/++	++/+++	+++	+++	+++	+++	++++
Hypothalamus	++	++	+/++	++/+++	+++	+++	+++	+++	++++
Cerebellum	+/++	+/++	+/++	+/++/+++	+/++/+++	++++	++++	++++	++++
Hippocampus	++	+/++	+/++	+/++/+++	+/++/+++	++/++++	+++/++++	+++/++++	++++
Motor cortex	+/++	+/++/+++	+/++/+++	+/++/+++	+/++/+++	++/+++/++++	+++/++++	+++/++++	+++/++++
Sensory cortex	+/++	+/++/+++	+/++/+++	+/++/+++	+/++/+++	++/+++/++++	+++/++++	+++/++++	+++/++++
Piriform cortex	++	++	+/++	++/+++	++++	++++	++++	++++	++++

0: absent, +: nuclear staining, ++: diffuse nuclear staining, +++: minimum inclusions, ++++: dense inclusions.

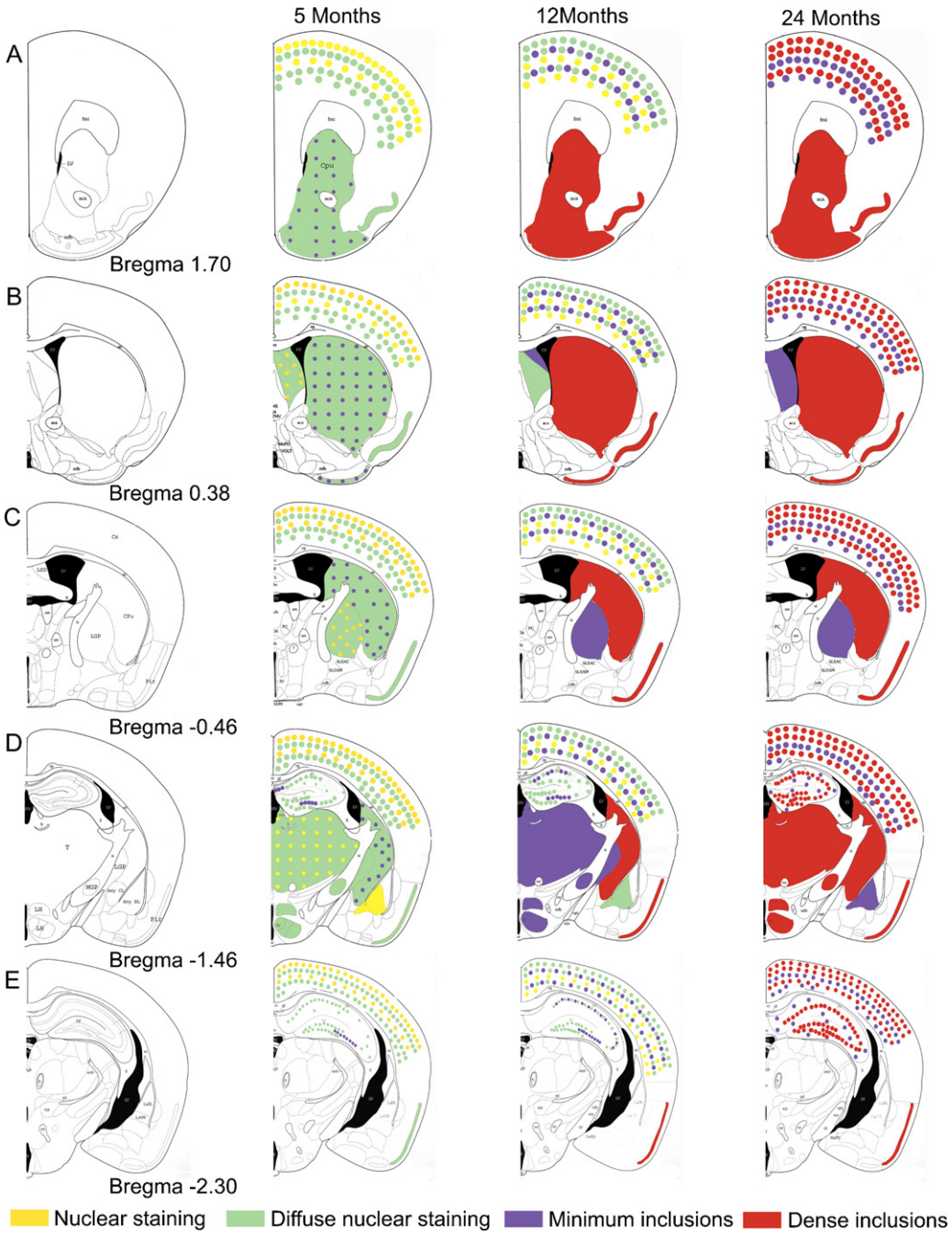

Fig. 2. Schematic overview of the spatial and temporal evolution of S830 immunostaining in *Hdh*$^{Q150/Q150}$ mouse brain at five coronal levels from anterior to posterior based on the atlas of Paxinos and Franklin (1997) [25] shown in the left column. Each subsequent column shows the S830 expression patterns for three time points 5, 12 and 24 months, respectively, using different colours. To indicate types of cellular pathology (see legend). Overlapping staining is represented by mixed colour. Abbreviations; Aca: anterior commissure, Amy BL: basolateral amygdale, Amy CL: central amygdala, cc: corpus callosum, CPu: caudate putamen, Cx: cortex, fmi: corpus callosum, GP: globus pallidus, LS: lateral septum, LSD: dorsal lateral septum, LGP: lateral globus pallidus, LV: lateral ventricle, Mfb: medial forebrain bundle, MGP: medial globus pallidus, Pir: piriform cortex, T: thalamus, Tu: olfactory tubercle.

homozygote mouse exhibited neuronal inclusions in the cytoplasm. These inclusions appeared as large circular filamentous structures with no membrane, but they were clearly distinguishable from their surrounding as a result of their high electron density (Fig. 6E). We were unable to determine small neuritic aggregates (ENNIs) by electron microscopy.

We also performed immunogold labelling of S830 antibody on the 14 month old and 21 month old homozygote knock-in mice. The immuno-reaction of mutant huntingtin was found to be specifically localised to the inside of the nuclear inclusion. The immunogold reactivity was confined to the filamentous bodies in the inside of nucleus and appeared as clusters of immunogold particles (Fig. 6C and F). No gold particles were seen in the negative control sections to which the application of primary antibody was omitted.

4. Discussion

All of the regions of the *Hdh*$^{Q150/Q150}$ brain examined showed diffuse nuclear staining and nuclear inclusions when immunolabelled with S830 antibody at 5 month of age. Low levels of both diffuse nuclear staining and NIIs were observed in the

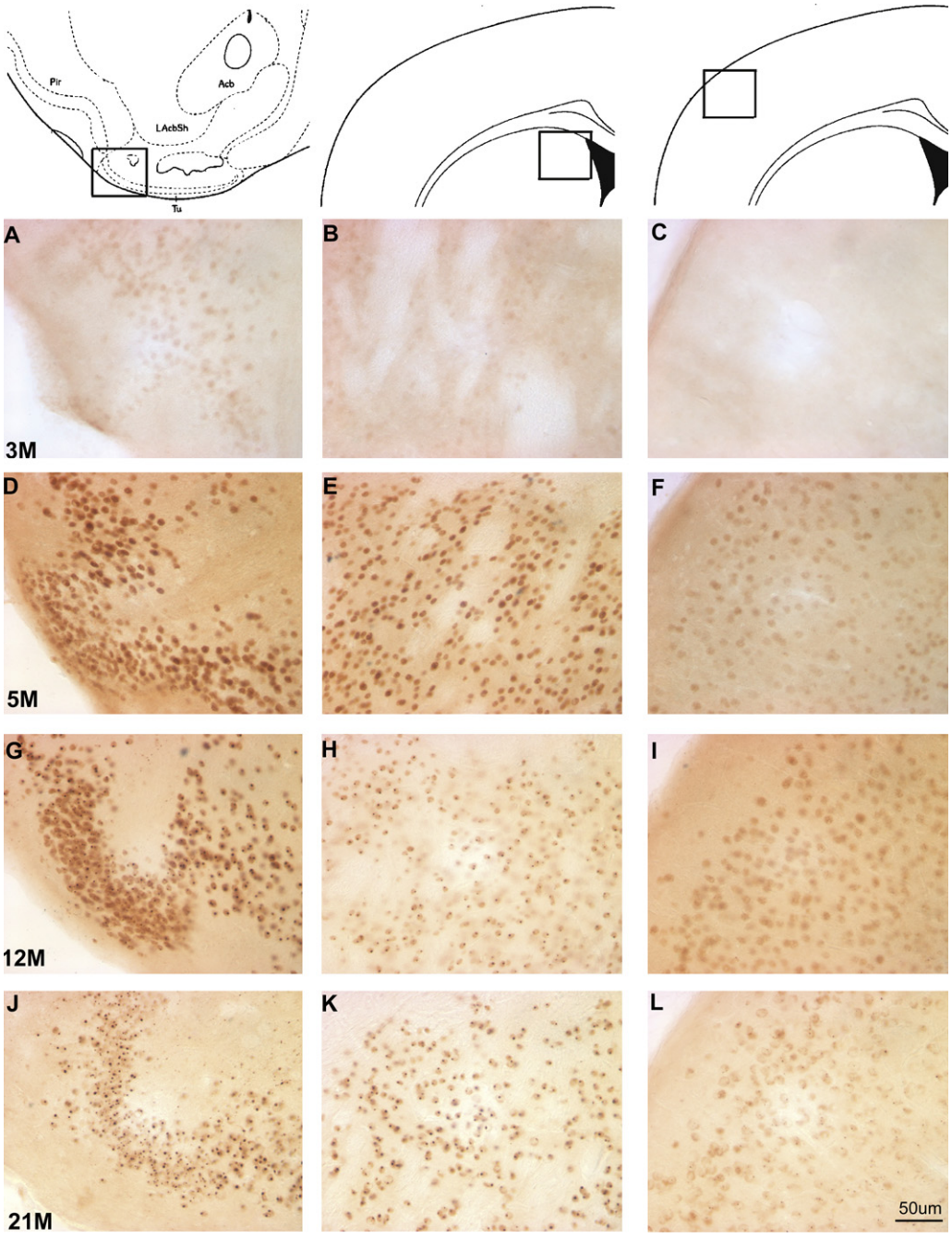

Fig. 3. Temporal evolution of S830 immunostaining of *Hdh*$^{Q150/Q150}$ brain in olfactory tubercle (left panels), striatum (middle panels), and cortex (right panels) at 3, 5, 12 and 21 months of age, in successive rows. The development of NIIs is clearly visible in olfactory tubercle and striatal cells.

olfactory tubercle, nucleus accumbens and striatum of young animals (5–12M). The 15 month old homozygote animals displayed NIIs in all regions of the brain with persistent diffuse nuclear staining, whereas by 18 months of age the mice no longer expressed diffuse nuclear immunoreactivity. This data suggests that the aggregation commences with the diffuse accumulation of protein in the nucleus, and as the phenotype progresses, these small diffuse concentrations are replaced by larger NII aggregates. Previous studies suggest mutant huntingtin may accumulate first in degenerating neurites and which then appear as a neuronal inclusion [33], or that they merge from individual aggregates into a single or several nuclear inclusions [14]. The latter description is more consistent with our study, which demonstrates that as the number of cells with inclusions increases, the number of cells with aggregations decreases. Consequently we report an inverse relationship between diffuse nuclear staining and inclusion number that is age dependant.

Tallaksen-Greene et al. [38] found in their histological studies on the *Hdh*$^{Q150/Q150}$ mice that huntingtin-associated NIIs were largely restricted to the striatum, with no evidence of gross neurodegeneration. The results of our study indicated that the nuclear inclusions can be present in all regions of the brain but that the distribution is age-dependent. The inclusions were found predominantly in the olfactory tubercle, nucleus accumbens, the striatum and central amygdala. Our study also demonstrated that nuclear inclusions were distributed widely in the striatum with persistent diffuse nuclear staining at 15 months old. This finding was consistent with that of Tallaksen-Greene et al. [38] who demonstrated

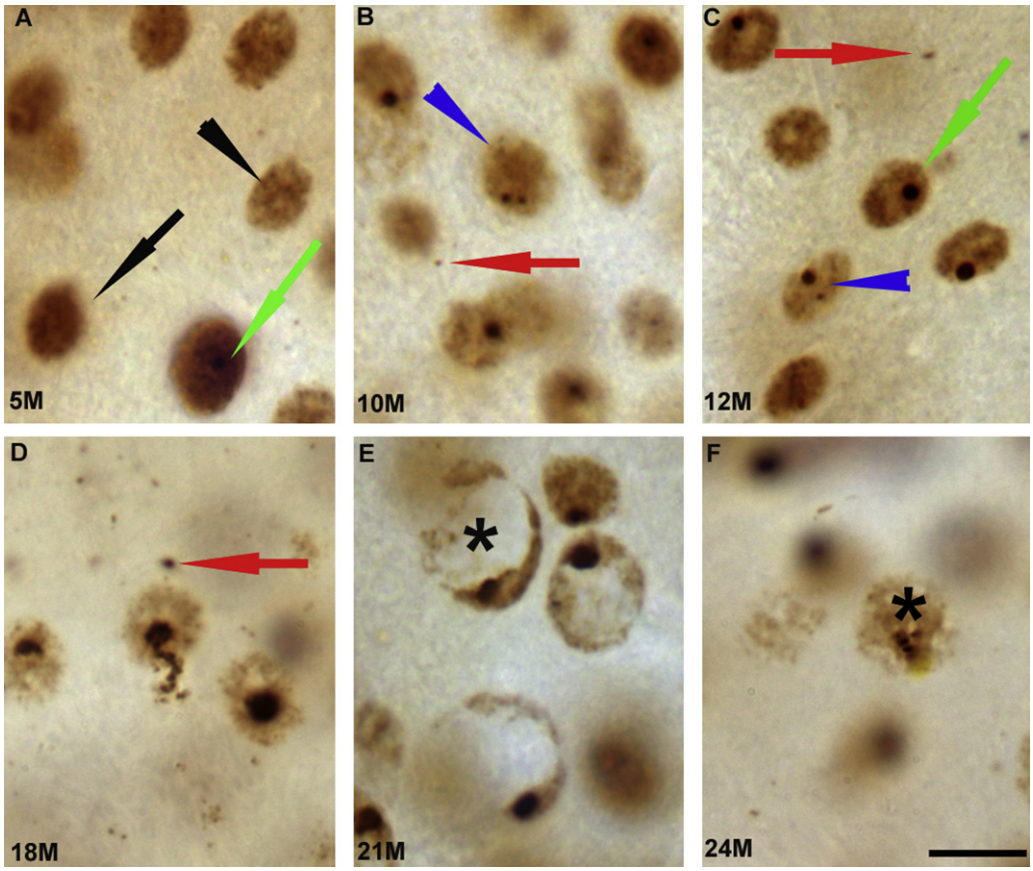

Fig. 4. High magnification images of striatal sections of *Hdh*$^{Q150/Q150}$ brain, showing age-dependent nuclear S830 immunoreactivity in 5 months through 24 months old mice (A–F). Both diffuse nucleus staining and nuclear inclusions are observed in animals aged 5, 10 and 12 months (A–C). Older animals display cells with diffuse nuclear staining together with nuclear inclusions (D–F), and these cells were widespread throughout the striatum at 21 months of age (E). The blue arrowheads denote cells with more than a single inclusion and the black arrow denotes diffuse nuclear staining. The green arrows indicate inclusions and the red arrows indicate extra nuclear inclusions. Scale bar = 10 μm. (For interpretation of the references to colour in this figure legend, the reader is referred to the web version of the article.)

that within the striatum, intra-nuclear huntingtin immunoreactivity was also observed from 6 months of age and that the diffuse staining persisted until 8 months [38]. We also observed diffuse nuclear staining in animals up to 12 months of age. With regard to the nuclear inclusions, the results of our study are consistent with those obtained by Tallaksen-Greene et al. [38] that showed nuclear inclusions were distributed widely throughout the striatum. By contrast, we did not find diffuse nuclear staining in aged animals. Another study by Woodman et al. [47] found evidence of NIIs in the striatum and hippocampus by 6 months of age and in the cortex by 8 months of age in the*Hdh*$^{Q150/Q150}$ mice, which may be due to the differences in the penetrance of the background strains used [47]. In contrast, we were able to observe NIIs in the olfactory tubercle, nucleus accumbens and striatum of 5 months old *Hdh*$^{Q150/Q150}$ mice. It has been reported that *Hdh*$^{(CAG)Q150}$ mice exhibits a reduction in striatal neuron numbers and in striatal

Table 2
Hdh$^{Q150/Q150}$ knock-in mice. Formation, progression and distribution of extra-nuclear inclusions (ENNIs).

Q150 brain/ages	5M	6M	8M	10M	12M	15M	18M	21M	24M
Olfactory tubercle	+	+/++	+	+/++	+++	++++	++++	++++	++++
Nucleus accumbens	+	+/++	+	+/++	++	+++	++++	++++	++++
Globus pallidus-lateral	+	+/++	+	+/++	+++	+++	++++	++++	++++
Globus pallidus-medial	+	+/++	+	+/++	+++	+++	++++	++++	++++
Striatum ventral	+	+/++	+	+/++	++	+++	+++	++++	++++
Striatum dorsal	+	+/++	+	+/++	++	+++	+++	++++	++++
Striatum posterior	+	+/++	+	+/++	++	+++	+++	++++	++++
Septum lateral	+	+/++	+	+/++	++	+++	+++	+++	+++
Septum med	+	+/++	+	+/++	+++	+++	+++	+++	+++
Amygdala BL	+	+/++	+	+/++	++	++	++	++	++
Amygdala CL	+	+/++	+	+/++	+++	+++	+++	++++	+++
Thalamus	+	+/++	+	+/++	++	++	+++	+++	++++
Hypothalamus	+	+/++	+	+/++	++	++	+++	+++	++++
Cerebellum	+	+/++	+	+/++	+++	++++	++++	++++	++++
Hippocampus	+	+/++	+	+/++	++	++	++	++	++
Motor cortex	+	+/++	+	+/++	++	++	+++	+++	+++
Sensory cortex	+	+/++	+	+/++	++	++	+++	+++	+++
Piriform cortex	+	+/++	+	+/++	+++	+++	++++	++++	++++

0: absent, +: very low staining, ++: intermediate staining, +++: dense staining, ++++: very dense staining.

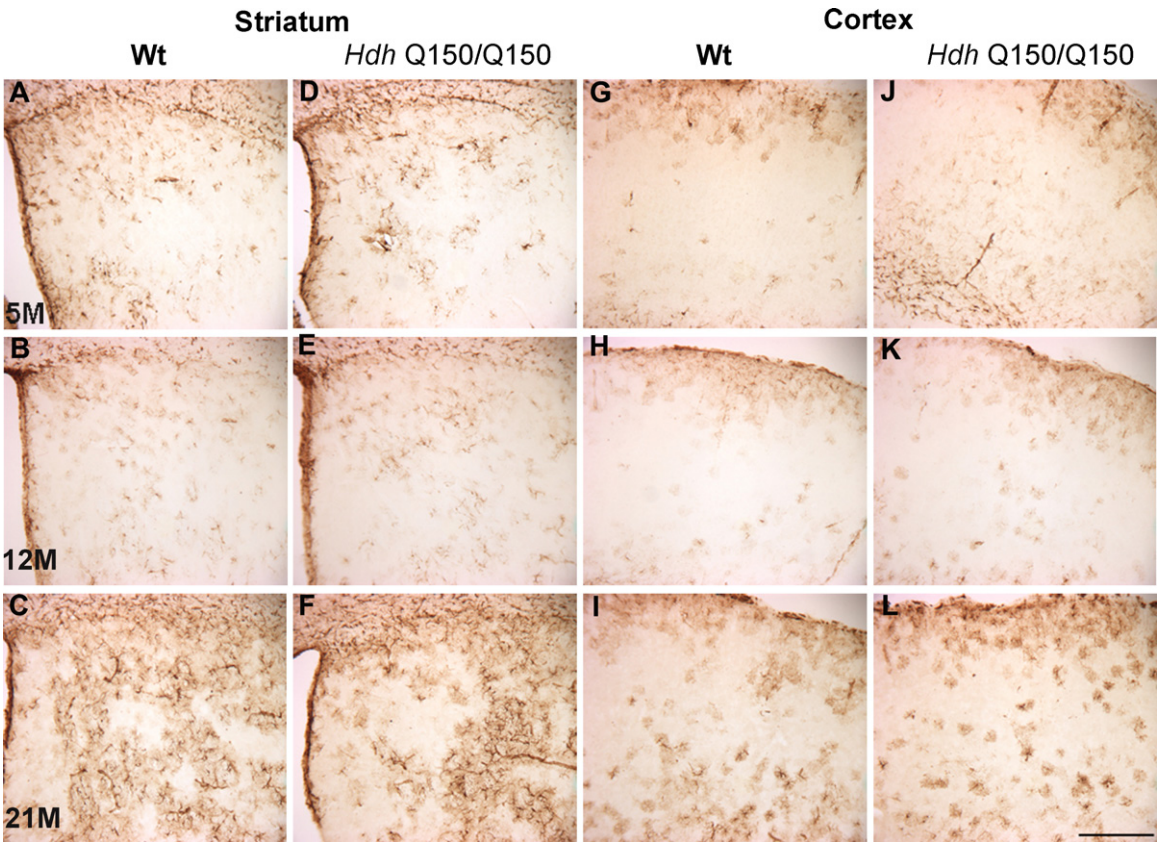

Fig. 5. Photomicrographs show the GFAP immunoreactive astrocytes in the striatum and cortex of the wildtype and *Hdh*$^{Q150/Q150}$ animals. (A–C) and (G–I) represent wildtype mice; (D–F) and (J–L) represent the *Hdh*$^{Q150/Q150}$ mouse. First row embody: 5 months old age; second row, 12 months old and third row, 21 months old, respectively. Scale bar = 100 μm.

volume at approximately 23 months of age [13]. A recent paper found no decrease in striatal volume or striatal neurons in the HdhQ200 mice [12], however, in the current study we have observed reduced striatal volume and striatal neuron numbers at 6 months of age. This may be due to the differences in the background.

Gutekunst et al. [11] have used the EM48 antibody which was raised against the first 256 amino acids of huntingtin and selectively recognizes aggregated huntingtin, to reveal more aggregates in the cortex than in striatum in the post mortem human HD brain. This observation is not reflected in our findings, in the *Hdh*$^{Q150/Q150}$ knock-in mouse line, where the striatum exhibited a greater number of aggregates than in the cortex. Our findings are consistent with other neuropathological studies in the HD mouse models [16,17,46] and represents one of the key differences between the human condition and the genetic mouse models. The light microscopy presented in the present study however, does reflect the pattern of aggregate distribution in different regions of HD human brain, for example in the caudate, putamen, substantia nigra, hypothalamic nuclei, thalamus, where aggregates are found in the human but at lower densities than in the cortex. At a cellular level, Gutekunst et al. [11] also described different localization of EM48-labelling in the HD cortical neurons. The EM48-labelled aggregates were found in the neuropil, in neuronal nuclei and perikarya, conversely we did not observe S830-labelling in the perikarya in the *Hdh*$^{Q150/Q150}$ mouse line, which may reflect differences in the antibodies.

Based on the results of our investigation, we further reveal that the extra-nuclear inclusions existed in all age groups from 5 months of age onwards. The ENNIs were found to be distributed throughout the brain in animals up to 10 months old. At 12 month the distribution of the immunoreaction products varied depending on the region of the brain. The globus pallidus, amygdala and piriform cortex, show increased intensity of extra-nuclear inclusions whereas other areas of the brain remained the same. Older homozygous mice of 21 and 24 months of age show the presence of these inclusions in all regions of the brain, but more densely than seen prior to 10 months of age. Morton et al. [22] showed that there is a progressive appearance of NIIs and ENNIs in striatum, cortex and hippocampus of R6/2 transgenic mice, with ubiquitin antibody [22]. In these R/2 mice there were two distinctly separate populations of inclusions, NIIs and ENNIs. We have also observed extra diffuse nuclear staining in the present study. Unlike Morton et al., we were not able to detect any ENNIs in the synaptic dendrites of the neurons by electron microscopy at any age. This may due to different antibodies used to detect inclusions, methodological differences between laboratories or differences in the mouse lines, as the R6/2 transgenic mice have a more rapidly progressing and severe phenotype than that seen in the *Hdh*$^{Q150/Q150}$ knock-in line.

In the present study, our TEM data in the *Hdh*$^{Q150/Q150}$ mouse line is in broad agreement with previous reports in the post-mortem of HD brains and transgenic mouse models, where intra-nuclear inclusions consist of filamentous structures [7,8,11,23]. In early studies, HD patient brains show nuclear membrane indentations, nuclear disorganization, reduction of the ribosomes [29,30], large accumulations of lipofucsin granules and enlarged mitochondria [39] at the ultrastructural level. Our findings show similar characteristic features in the *Hdh*$^{Q150/Q150}$ mouse. Yu et al. [48] found that the striatal neurons of 14 month *Hdh*$^{Q150/Q150}$ mice showed markers of cytoplasmic degeneration such as cytoplasmic swelling, vacuolization, enlargement and degenerated mitochondria. In the present study these were absent in 14 month old animals. However, they were present in the 21 month old

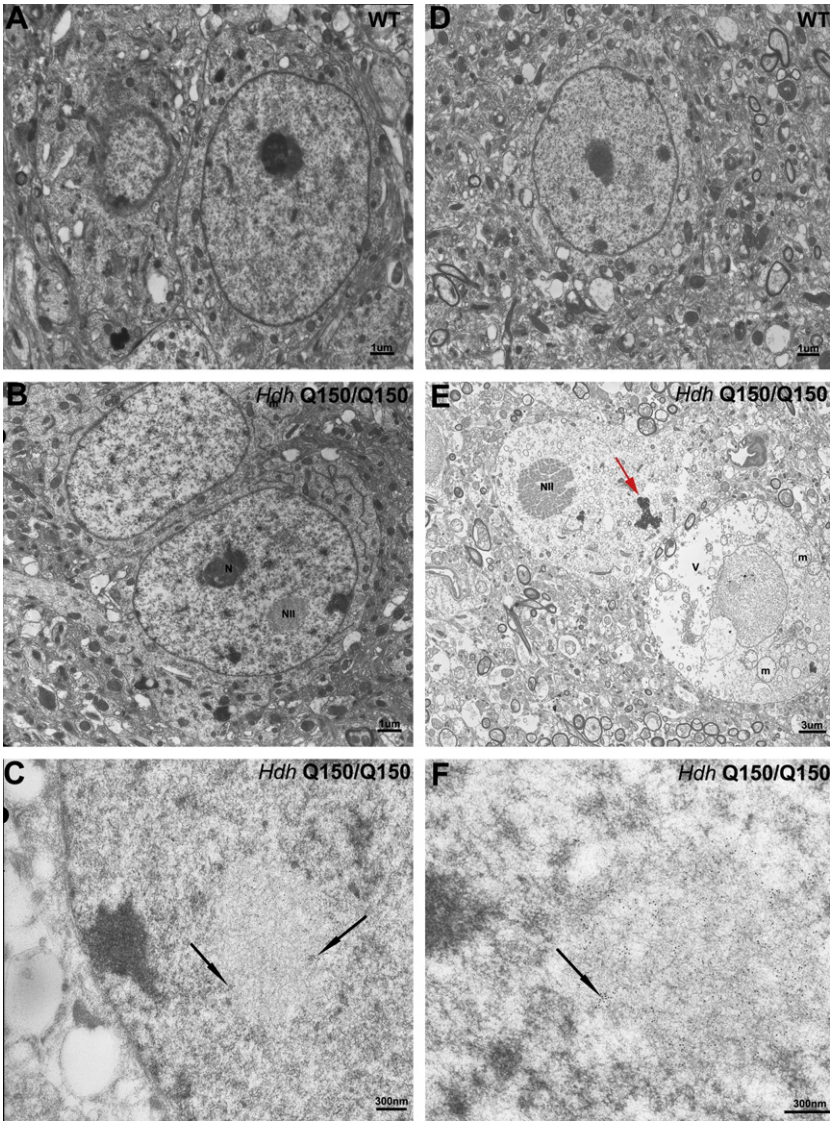

Fig. 6. TEM and immunogold images of the striatum of $Hdh^{Q150/Q150}$ (B, C, E and F) and wildtype mice (A and D) at 14 and 21 months of age. Left panel represents 14 months; right panel represents 21 months of age. Nuclear inclusions are observed in both 14 months (B) and 21 months (E) with electron microscope. Hypertrophic neuronal degeneration as shown by loss of cytoplasmic contents such as mitochondria (m) and large vacuolization (v) in noted in older $Hdh^{Q150/Q150}$ (E). S830 immunogold labelled particles are localised in intra-nuclear inclusions as shown by black arrows in 14 months (C) and 21 months old (F) animals. WT: wildtype, Hdh CAG (150): $Hdh^{Q150/Q150}$, N: nucleolus, NII: intra-nuclear inclusion, red arrow: electron dense body. Magnifications are as described in figures. (For interpretation of the references to colour in this figure legend, the reader is referred to the web version of the article.)

$Hdh^{Q150/Q150}$ mice. Moreover, our results revealed that immunogold particles were only confined to the intra-nuclear inclusions. In contrast to our finding, Yu et al. [48] detected immunogold particles that were either clustered within the degenerating mitochondria or associated with the mitochondrial membrane [48]. Similarly Panov et al. [24] showed with electron microscopy, that mutant huntingtin is also localized on the mitochondrial membrane of the cells in YAC72 transgenic mice [24]. The differences in location of immunogold particles may be due to the antibody used, the precise histochemical and ultrastructural methods and/or the mouse strain. Mutant huntingtin aggregates were also observed in hypertrophic and dark glial cells with no visible cytoplasmic organelles in the striatum of R6/2 mice at 12 weeks with EM48 antibody by TEM [35]. In agreement, we have found hypertrophic cells with no visible cytoplasmic organelles also in the $Hdh^{Q150/Q150}$ mice. A recent study found that nuclear pore complexes deteriorate in aged mice. In old neurons, this progression leads to an increased nuclear permeability and causes a leakage of cytoplasmic proteins into the nucleus. It has also been revealed that cytoplasmic proteins such as intra-nuclear tubulin aggregates into large filamentous structures which caused severe morphological chromatin abnormalities [5]. This supports the idea, that the $Hdh^{Q150/Q150}$ mice had uneven nuclear membrane suggesting a possible deterioration of the nuclear pore complexes in HD.

Interestingly, we did not find any alteration in the intensity of GFAP immunostaining between $Hdh^{Q150/Q150}$ homozygous and their littermates. This finding contradicts the result of Lin et al. [17] and Yu et al. [48], who studied the same $Hdh^{Q150/Q150}$ knock-in mouse line and found increased GFAP activity at 14 months of age. This may indicate that astroglial reaction was not associated with the expanded CAG repeat length.

In running longitudinal studies of this nature several technical difficulties arose, most notably regarding the consistency of staining. At the 8 month time point we lost some consistency of the S830 staining which impacted on our S830 cell counts but also on our 8 month cresyl violet counts. We also had a tissue processing failure

in 5 months of age which may have resulted in artificially low cell counts. These problems resulted in slightly disproportionate counts compared with adjacent date sets, but we included counts in the final data sets, as they are still representative of the animals used.

Here, we have shown that a marked and progressive cellular phenotype is present in the *Hdh*$^{Q150/Q150}$ mouse model. Diffuse nuclear staining and inclusions are first observed at 5 months and progress with age. The *Hdh*$^{Q150/Q150}$ mice show reduced striatal volume compared to the wildtypes. Our data confirms that the *Hdh*$^{Q150/Q150}$ mice show cell pathology similar to those obtained from post-mortem brains of HD patients.

Acknowledgements

We thank Prof Gillian Bates (King College London) for the generous gift of S830 antibody. We also thank Prof I for Bowen and Dr Antony Hann (Cardiff University) for helpful advice on implementation of the EM studies and Ali Baird, Jane Heath and Linda Elliston for technical support. This work was funded by the Medical Research Council of the UK and Cure Huntington's Disease Intuitive (CHDI) Foundation Inc..

References

[1] M. Abercrombie, Estimation of nuclear population from microtome sections, Anat. Rec. (1946) 239–247.
[2] G.P. Bates, P.S. Harper, L. Jones, in: G.P. Bates, P.S. Harper, L. Jones (Eds.), Huntington's Disease, vol. 5, Oxford University Press, 2002.
[3] A. Bignami, L.F. Eng, D. Dahl, C.T. Uyeda, Localization of the glial fibrillary acidic protein in astrocytes by immunofluorescence, Brain Res. 43 (1972) 429–435.
[4] S. Brooks, G. Higgs, L. Jones, S.B. Dunnett, Longitudinal analysis of the behavioural phenotype in Hdh((CAG)150) Huntington's disease knock-in mice, Brain Res. Bull. 88 (2012) 182–188.
[5] M.A. D'Angelo, M. Raices, S.H. Panowski, M.W. Hetzer, Age-dependent deterioration of nuclear pore complexes causes a loss of nuclear integrity in postmitotic cells, Cell 136 (2009) 284–295.
[6] D. Dahl, A. Bignami, K. Weber, M. Osborn, Filament proteins in rat optic nerves undergoing Wallerian degeneration: localization of vimentin, the fibroblastic 100-A filament protein, in normal and reactive astrocytes, Exp. Neurol. 73 (1981) 496–506.
[7] S.W. Davies, M. Turmaine, B.A. Cozens, M. DiFiglia, A.H. Sharp, C.A. Ross, E. Scherzinger, E.E. Wanker, L. Mangiarini, G.P. Bates, Formation of neuronal intranuclear inclusions underlies the neurological dysfunction in mice transgenic for the HD mutation, Cell 90 (1997) 537–548.
[8] M. DiFiglia, E. Sapp, K.O. Chase, S.W. Davies, G.P. Bates, J.P. Vonsattel, N. Aronin, Aggregation of huntingtin in neuronal intranuclear inclusions and dystrophic neurites in brain, Science 277 (1997) 1990–1993.
[9] R.J. Ferrante, N.W. Kowall, M.F. Beal, E.P. Richardson Jr., E.D. Bird, J.B. Martin, Selective sparing of a class of striatal neurons in Huntington's disease, Science 230 (1985) 561–563.
[10] S. Galatioto, Immunohistochemical findings in Huntington's Chorea: report of 9 cases, Pathologica 88 (1996) 491–499.
[11] C.A. Gutekunst, S.H. Li, H. Yi, J.S. Mulroy, S. Kuemmerle, R. Jones, D. Rye, R.J. Ferrante, S.M. Hersch, X.J. Li, Nuclear and neuropil aggregates in Huntington's disease: relationship to neuropathology, J. Neurosci. 19 (1999) 2522–2534.
[12] M.Y. Heng, D.K. Duong, R.L. Albin, S.J. Tallaksen-Greene, J.M. Hunter, M.J. Lesort, A. Osmand, H.L. Paulson, P.J. Detloff, Early autophagic response in a novel knock-in model of Huntington disease, Hum. Mol. Genet. 19 (2010) 3702–3720.
[13] M.Y. Heng, S.J. Tallaksen-Greene, P.J. Detloff, R.L. Albin, Longitudinal evaluation of the Hdh(CAG)150 knock-in murine model of Huntington's disease, J. Neurosci. 27 (2007) 8989–8998.
[14] R.R. Kopito, Aggresomes, inclusion bodies and protein aggregation, Trends Cell Biol. 10 (2000) 524–530.
[15] H. Li, S.H. Li, A.L. Cheng, L. Mangiarini, G.P. Bates, X.J. Li, Ultrastructural localization and progressive formation of neuropil aggregates in Huntington's disease transgenic mice, Hum. Mol. Genet. 8 (1999) 1227–1236.
[16] H. Li, S.H. Li, H. Johnston, P.F. Shelbourne, X.J. Li, Amino-terminal fragments of mutant huntingtin show selective accumulation in striatal neurons and synaptic toxicity, Nat. Genet. 25 (2000) 385–389.
[17] C.H. Lin, S. Tallaksen-Greene, W.M. Chien, J.A. Cearley, W.S. Jackson, A.B. Crouse, S. Ren, X.J. Li, R.L. Albin, P.J. Detloff, Neurological abnormalities in a knock-in mouse model of Huntington's disease, Hum. Mol. Genet. 10 (2001) 137–144.
[18] A. Lunkes, J.L. Mandel, A cellular model that recapitulates major pathogenic steps of Huntington's disease, Hum. Mol. Genet. 7 (1998) 1355–1361.
[19] V. Macdonald, G. Halliday, Pyramidal cell loss in motor cortices in Huntington's disease, Neurobiol. Dis. 10 (2002) 378–386.
[20] L. Mangiarini, K. Sathasivam, M. Seller, B. Cozens, A. Harper, C. Hetherington, M. Lawton, Y. Trottier, H. Lehrach, S.W. Davies, G.P. Bates, Exon 1 of the HD gene with an expanded CAG repeat is sufficient to cause a progressive neurological phenotype in transgenic mice, Cell 87 (1996) 493–506.
[21] A.J. Milnerwood, D.M. Cummings, G.M. Dallerac, J.Y. Brown, S.C. Vatsavayai, M.C. Hirst, P. Rezaie, K.P. Murphy, Early development of aberrant synaptic plasticity in a mouse model of Huntington's disease, Hum. Mol. Genet. 15 (2006) 1690–1703.
[22] A.J. Morton, M.A. Lagan, J.N. Skepper, S.B. Dunnett, Progressive formation of inclusions in the striatum and hippocampus of mice transgenic for the human Huntington's disease mutation, J. Neurocytol. 29 (2000) 679–702.
[23] J.M. Ordway, S. Tallaksen-Greene, C.A. Gutekunst, E.M. Bernstein, J.A. Cearley, H.W. Wiener, L.S. Dure, R. Lindsey, S.M. Hersch, R.S. Jope, R.L. Albin, P.J. Detloff, Ectopically expressed CAG repeats cause intranuclear inclusions and a progressive late onset neurological phenotype in the mouse, Cell 91 (1997) 753–763.
[24] A.V. Panov, C.A. Gutekunst, B.R. Leavitt, M.R. Hayden, J.R. Burke, W.J. Strittmatter, J.T. Greenamyre, Early mitochondrial calcium defects in Huntington's disease are a direct effect of polyglutamines, Nat. Neurosci. 5 (2002) 731–736.
[25] G. Paxinos, K.B.J. Franklin, The Mouse Brain in Stereotaxic Coordinates, 2nd ed., Academic Press, San Diego CA, 2001.
[26] P.H. Reddy, M. Williams, V. Charles, L. Garrett, L. Pike-Buchanan, W.O. Whetsell Jr., G. Miller, D.A. Tagle, Behavioural abnormalities and selective neuronal loss in HD transgenic mice expressing mutated full-length HD cDNA, Nat. Genet. 20 (1998) 198–202.
[27] P.H. Reddy, M. Williams, D.A. Tagle, Recent advances in understanding the pathogenesis of Huntington's disease, Trends Neurosci. 22 (1999) 248–255.
[28] A. Reiner, N. Del Mar, Y.P. Deng, C.A. Meade, Z. Sun, D. Goldowitz, R6/2 neurons with intranuclear inclusions survive for prolonged periods in the brains of chimeric mice, J. Comp. Neurol. 505 (2007) 603–629.
[29] R.A. Roos, G.T. Bots, Nuclear membrane indentations in Huntington's chorea, J. Neurol. Sci. 61 (1983) 37–47.
[30] R.A. Roos, J.F. Pruyt, J. de Vries, G.T. Bots, Neuronal distribution in the putamen in Huntington's disease, J. Neurol. Neurosurg. Psychiatry 48 (1985) 422–425.
[31] H.D. Rosas, A.K. Liu, S. Hersch, M. Glessner, R.J. Ferrante, D.H. Salat, K.A. van der, B.G. Jenkins, A.M. Dale, B. Fischl, Regional and progressive thinning of the cortical ribbon in Huntington's disease, Neurology 58 (2002) 695–701.
[32] C.A. Ross, Intranuclear neuronal inclusions: a common pathogenic mechanism for glutamine-repeat neurodegenerative diseases? Neuron 19 (1997) 1147–1150.
[33] E. Sapp, C. Schwarz, K. Chase, P.G. Bhide, A.B. Young, J. Penney, J.P. Vonsattel, N. Aronin, M. DiFiglia, Huntingtin localization in brains of normal and Huntington's disease patients, Ann. Neurol. 42 (1997) 604–612.
[34] F. Saudou, S. Finkbeiner, D. Devys, M.E. Greenberg, Huntingtin acts in the nucleus to induce apoptosis but death does not correlate with the formation of intranuclear inclusions, Cell 95 (1998) 55–66.
[35] J.Y. Shin, Z.H. Fang, Z.X. Yu, C.E. Wang, S.H. Li, X.J. Li, Expression of mutant huntingtin in glial cells contributes to neuronal excitotoxicity, J. Cell Biol. 171 (2005) 1001–1012.
[36] S.K. Singhrao, P. Thomas, J.D. Wood, J.C. MacMillan, J.W. Neal, P.S. Harper, A.L. Jones, Huntingtin protein colocalizes with lesions of neurodegenerative diseases: an investigation in Huntington's, Alzheimer's, and Pick's diseases, Exp. Neurol. 150 (1998) 213–222.
[37] S.S. Sisodia, Nuclear inclusions in glutamine repeat disorders: are they pernicious, coincidental, or beneficial? Cell 95 (1998) 1–4.
[38] S.J. Tallaksen-Greene, A.B. Crouse, J.M. Hunter, P.J. Detloff, R.L. Albin, Neuronal intranuclear inclusions and neuropil aggregates in HdhCAG(150) knockin mice, Neuroscience 131 (2005) 843–852.
[39] I. Tellez-Nagel, A.B. Johnson, R.D. Terry, Studies on brain biopsies of patients with Huntington's chorea, J. Neuropathol. Exp. Neurol. 33 (1974) 308–332.
[40] The Huntington's Disease Collaborative Research Group, A novel gene containing a trinucleotide repeat that is expanded and unstable on Huntington's disease chromosomes, Cell 72 (1993) 971–983.
[41] R.C. Trueman, S.P. Brooks, L. Jones, S.B. Dunnett, The operant serial implicit learning task reveals early onset motor learning deficits in the Hdh knock-in mouse model of Huntington's disease, Eur. J. Neurosci. 25 (2007) 551–558.
[42] M. Turmaine, A. Raza, A. Mahal, L. Mangiarini, G.P. Bates, S.W. Davies, Nonapoptotic neurodegeneration in a transgenic mouse model of Huntington's disease, Proc. Natl. Acad. Sci. U.S.A. 97 (2000) 8093–8097.
[43] J.C. Vis, L.F. Nicholson, R.L. Faull, W.H. Evans, N.J. Severs, C.R. Green, Connexin expression in Huntington's diseased human brain, Cell Biol. Int. 22 (1998) 837–847.
[44] J.P. Vonsattel, M. DiFiglia, Huntington disease, J. Neuropathol. Exp. Neurol. 57 (1998) 369–384.
[45] J.P. Vonsattel, R.H. Myers, T.J. Stevens, R.J. Ferrante, E.D. Bird, E.P. Richardson Jr., Neuropathological classification of Huntington's disease, J. Neuropathol. Exp. Neurol. 44 (1985) 559–577.
[46] V.C. Wheeler, J.K. White, C.A. Gutekunst, V. Vrbanac, M. Weaver, X.J. Li, S.H. Li, H. Yi, J.P. Vonsattel, J.F. Gusella, S. Hersch, W. Auerbach, A.L. Joyner, M.E. MacDonald, Long glutamine tracts cause nuclear localization of a novel form of huntingtin in medium spiny striatal neurons in HdhQ92 and HdhQ111 knock-in mice, Hum. Mol. Genet. 9 (2000) 503–513.
[47] B. Woodman, R. Butler, C. Landles, M.K. Lupton, J. Tse, E. Hockly, H. Moffitt, K. Sathasivam, G.P. Bates, The Hdh(Q150/Q150) knock-in mouse model of HD and the R6/2 exon 1 model develop comparable and widespread molecular phenotypes, Brain Res. Bull. 72 (2007) 83–97.
[48] Z.X. Yu, S.H. Li, J. Evans, A. Pillarisetti, H. Li, X.J. Li, Mutant huntingtin causes context-dependent neurodegeneration in mice with Huntington's disease, J. Neurosci. 23 (2003) 2193–2202.